The Journal of Chemical Physics

# Light-controlled assembly of active colloidal molecules

Cite as: J. Chem. Phys. **150**, 094905 (2019); https://doi.org/10.1063/1.5079861
Submitted: 04 November 2018 . Accepted: 30 January 2019 . Published Online: 07 March 2019

Falko Schmidt, Benno Liebchen, Hartmut Löwen, and Giovanni Volpe

The Journal of Chemical Physics ARTICLE scitation.org/journal/jcp

# Light-controlled assembly of active colloidal molecules

Cite as: J. Chem. Phys. 150, 094905 (2019); doi: 10.1063/1.5079861
Submitted: 4 November 2018 • Accepted: 30 January 2019 •
Published Online: 7 March 2019



Falko Schmidt,[1,a)] Benno Liebchen,[2,a)] Hartmut Löwen,[2,b)] and Giovanni Volpe[1,c)]

## AFFILIATIONS

[1] Department of Physics, University of Gothenburg, SE-41296 Gothenburg, Sweden
[2] Institut für Theoretische Physik II: Weiche Materie, Heinrich-Heine-Universität Düsseldorf, D-40225 Düsseldorf, Germany

**Note:** This article is part of the Special Topic "Chemical Physics of Active Matter" in J. Chem. Phys.
[a)] **Contributions:** F. Schmidt and B. Liebchen contributed equally to this work.
[b)] **Electronic mail:** hlowen@hhu.de
[c)] **Electronic mail:** giovanni.volpe@physics.gu.se

## ABSTRACT

Thanks to a constant energy input, active matter can self-assemble into phases with complex architectures and functionalities such as living clusters that dynamically form, reshape, and break-up, which are forbidden in equilibrium materials by the entropy maximization (or free energy minimization) principle. The challenge to control this active self-assembly has evoked widespread efforts typically hinging on engineering of the properties of individual motile constituents. Here, we provide a different route, where activity occurs as an emergent phenomenon only when individual building blocks bind together in a way that we control by laser light. Using experiments and simulations of two species of immotile microspheres, we exemplify this route by creating active molecules featuring a complex array of behaviors, becoming migrators, spinners, and rotators. The possibility to control the dynamics of active self-assembly via light-controllable nonreciprocal interactions will inspire new approaches to understand living matter and to design active materials.



## I. INTRODUCTION

One promising approach to create functional materials as required by 21st century's technologies is provided by self-assembly. Here, a basic starting point is to explore and control the binding of particles in a molecule, which works in principle on all scales, from atoms to colloids. As compared to their atomistic counterparts, the formation of colloidal molecules[1–6] offers an enhanced control, based on the possibility to design their shapes and coatings on demand, as illustrated, e.g., by the admirable achievements on "patchy colloids."[1–4]

While many studies exploring the self-assembly of molecules focus on equilibrium systems, active particles that locally inject energy into a material open promising new horizons for self-assembly. These active particles are intrinsically away from thermal equilibrium,[7–10] which allows them to conquer a new level of complexity. This new complexity finds its perhaps most spectacular expression in the hierarchical self-organization of biological matter, often leading to functionalities such as clustering,[11] navigation,[12] self-healing,[13] or reproduction.[14] It has been recently theoretically suggested[15–17] that activity can also be exploited to form active molecules where the nonequilibrium settings allow the spontaneous emergence of new physical properties: the nonequilibrium chemical interaction between two immotile particles of different species will be generally nonreciprocal,[15] resulting in the formation of colloidal molecules that may spontaneously acquire motility.[16,17] This differs conceptually from active molecules involving components that are individually motile[18–23] and also from molecules that are first prepared with an irreversible bonding and then acquire motility as an independent additional effect in electric ac-fields.[24,25]

Here, we experimentally demonstrate the formation of light-controllable active colloidal molecules from a suspension

of light-absorbing and non-absorbing immotile microspheres immersed in a subcritical liquid mixture. When illuminated, the liquid surrounding the light-absorbing microparticles warms up. This temperature increase is isotropic and, therefore, does not lead to self-propulsion of the light-absorbing particles, different from previous work on light-activated colloids;[26] however, it induces attraction among nearby colloids, which come together because of phoretic interactions at intermediate interparticle distances[26–28] (probably thermophoresis) and stick together because of short range attractions (probably van der Waals and perhaps critical Casimir forces).[29–31] For example, a Janus dimer is formed when this light-induced attraction holds a non-absorbing microsphere and an absorbing one together. This dimer experiences a temperature gradient and moves phoretically.[32–38] When more microspheres come together, they form more complex molecules including stators, migrators, spinners, and rotators. Importantly, we remark that the emergence of directed motion of two binding immotile particles is not an obvious consequence of symmetry breaking—rather, it is forbidden in equilibrium on the relevant scales and crucially exploits the presence of a nonequilibrium environment. The striking new feature of the present approach is that motility occurs as an emergent nonequilibrium phenomenon from particle interactions that are controllable by light. This establishes a generic route to control nonreciprocal interactions among colloids by light, which is based on the laser-stimulated production of a phoretic field (e.g., chemicals, temperature, ions) by one species that attracts another species without causing a counteraction. This route offers control of the dynamics of active molecule formation, which can be switched on, off, paused or resumed on demand, and can be used to statistically control the composition of the system, e.g., with respect to the ratio of linear and chiral swimmers, as we demonstrate below. Remarkably, also the concept of emergent motility itself may inspire new collective phenomena beyond those featured by individually motile particles.[26,39–44]

## II. RESULTS

### A. Experiments

We consider a mixture of light-absorbing and non-absorbing colloidal particles (radius $R \approx 0.49\ \mu$m) made of silica with and without iron-oxide inclusions in a near-critical water-lutidine mixture in a quasi two-dimensional sample chamber (see Appendix A for details). Both species of particles settle down above the bottom wall of the sample at approximately the same distance because their specific density and electrostatic interactions are similar; when compared with the same particles in the bulk of the solution, this increases the viscous drag acting on the particles by a constant factor,[45] but does not otherwise qualitatively alter their dynamics. Without illumination, both species show Brownian diffusion

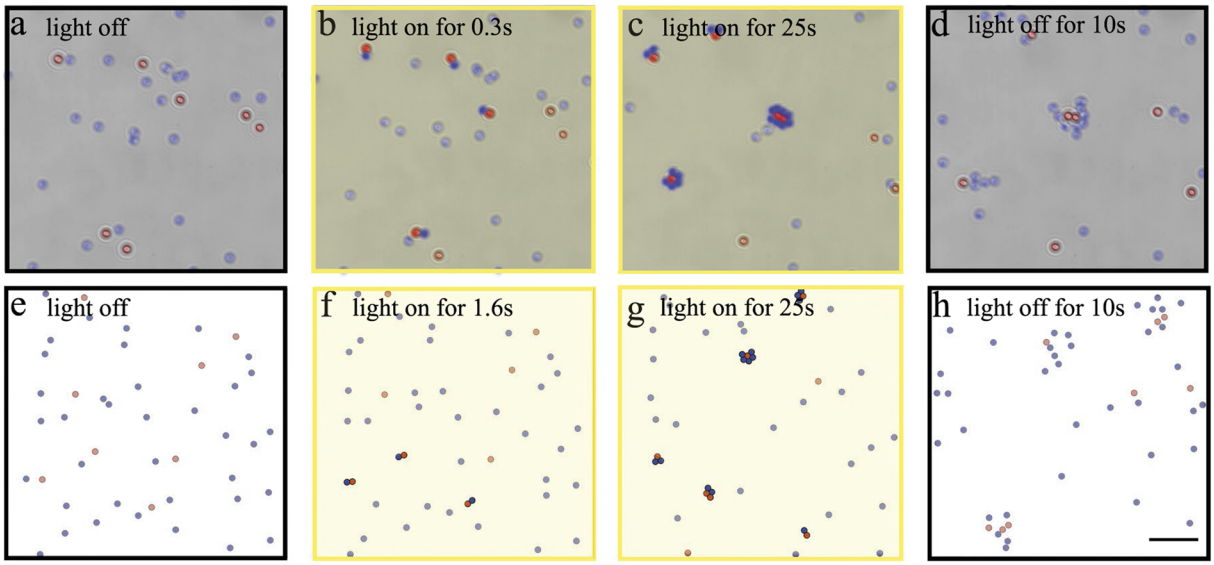


**FIG. 1. Spontaneous assembly of active colloidal molecules from immotile building blocks.** Series of snapshots from an experiment (top) and a simulation (bottom) [(a) and (e)]. Initially, there are building blocks of two non-interacting species: light-absorbing [red, Fig. 2(a)] and non-absorbing [blue, Fig. 2(b)] spherical colloidal particles, which perform standard Brownian motion. [(b) and (f)] When the sample is illuminated, the absorbing particles warm their surroundings, and when they randomly meet a non-absorbing particle, they join forming a self-propelling Janus dimer [Fig. 2(c)]. [(c) and (g)] As time passes, the dimers collect additional particles and more complex structures emerge, which feature more complex behaviors, such as *migrators* [Figs. 2(c)–2(e)], *stators* [Fig. 2(f)], *spinners* [Fig. 2(g)], and *rotators* [Fig. 2(h)]. [(d) and (h)] When the illumination is switched off, the active molecules disassemble and their component particles diffuse away. The simulations use 1 $\mu$m and 1 s as length and time units, respectively, and values of the particle radii, diffusion constants, and pair-molecule velocities as in the experiments (see Appendix B for a detailed discussion). The scale bar is 10 $\mu$m, and the laser intensity is $I = 80\ \mu\text{W}\ \mu\text{m}^{-2}$. Multimedia view: https://doi.org/10.1063/1.5079861.1

[Fig. 1(a) (Multimedia view)], as can also be seen from their trajectories [Figs. 2(a) and 2(b)]. However, when illuminated, the fluid heats up only in the vicinity of the light-absorbing particles so that the fluid locally demixes and induces attractive interactions with other particles in the vicinity. The strength of the attractive interactions increases when enhancing the laser power, while control experiments in water show that no molecules form. When an absorbing microsphere comes close to a non-absorbing one, we observe the formation of a heterogeneous dimer [Fig. 1(b) (Multimedia view)], which, unlike the colloidal building blocks it consists of, starts to move ballistically. This ballistic motion is forbidden in equilibrium and is therefore not a simple consequence of symmetry breaking, but also involves nonequilibrium fluctuations. In analogy to self-propelled Janus colloids, we call the emerging dimer a *Janus dimer*. Janus dimers represent the simplest active molecules. Their speed and rotational diffusion amounts to $v_2 = 2.0 \pm 0.4\ \mu\text{m s}^{-1}$ and $D_r = 0.11 \pm 0.05\ \text{s}^{-1}$. In the course of our experiments, the size of the molecules keeps on growing as time passes and clusters coalesce: the dimers move around and collect additional particles so that more complex structures emerge, which feature more complex behaviors, as shown in Fig. 1(c) (Multimedia view). These behaviors are intimately linked to the symmetry properties of the resulting active molecules. There are axis-symmetric molecules that behave as *migrators* performing linear active Brownian motion, such as dimers [Fig. 2(c)], trimers [Fig. 2(d)], as well as larger structures [Fig. 2(e)], which move with the absorbing microsphere in front.[34–38] More symmetric shapes perform standard Brownian motion, behaving as *stators* [i.e., passive colloidal molecules, Fig. 2(f)]. Finally, chiral shapes behave as either *spinners* [Fig. 2(g)] or *rotators* [Fig. 2(h)], featuring different forms of chiral active Brownian motion. Importantly, the assembly mechanism of these active molecules is fully reversible and they melt by thermal diffusion when the light is switched off [Fig. 1(d) (Multimedia view)]. The speed and rotation frequency of these molecules depend on the details

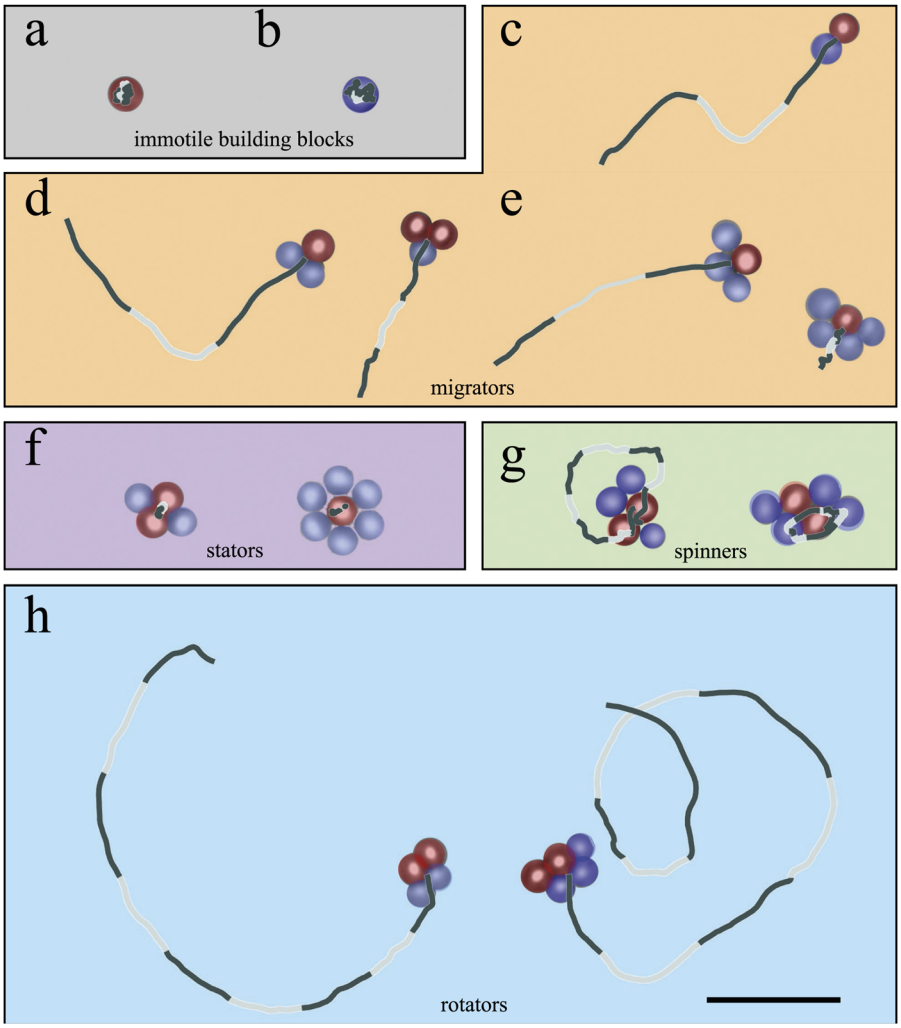


**FIG. 2. The zoological garden of active molecules.** While the constituting building blocks are immotile symmetric spherical (a) light-absorbing and (b) non-absorbing particles, the emerging active molecules present more and more complex shapes and behaviors as time evolves. We observe (c) dimers, (d) trimers, and (e) more complex axis-symmetric active molecules, which perform linear active Brownian motion (*migrators*); (f) highly symmetric molecules that do not show activity (*stators*); (g) rotationally symmetric chiral active molecules which rotate almost without translating (*spinners*); and (h) asymmetric chiral active molecules which swim in circles (*rotators*). In all cases, lines represent particle trajectories; grey and black segments correspond to 1-s stretches. The scale bar is 5 $\mu$m.

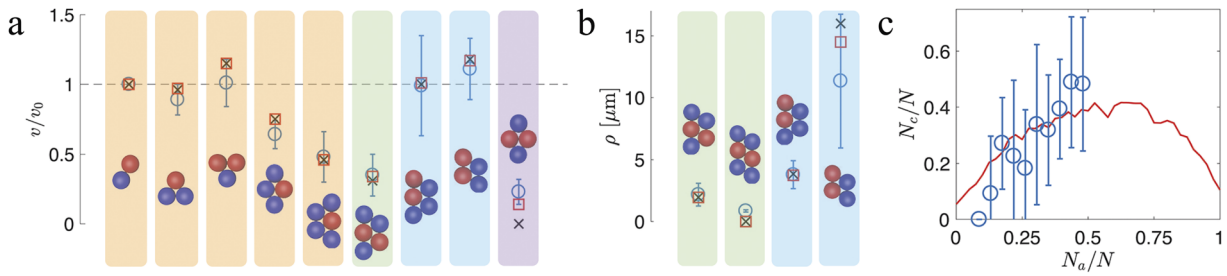


**FIG. 3. Quantitative agreement between experiments, simulations, and analytical predictions.** (a) The speed $v$ (normalized by the speed of the dimer $v_0$) and (b) swimming radius $\rho$ of active molecules obtained experimentally from the measured trajectories (blue circles and relative error bars representing a standard deviation), numerically from the simulated trajectories (red squares), and analytically for $D = 0$ from Eqs. (B7) and (B8) (black crosses) are all in good agreement. The molecules are given colored backgrounds depending on their classification reported in Fig. 2. (c) Chirality control: The fraction of chiral active molecules ($N_c/N$) can be controlled by the fraction of absorbing particles ($N_a/N$) in the initial suspension. The blue circles and relative error bars representing a standard deviation are the experimental data, and the red solid line represents the simulation results. Simulation parameters in Appendix B.

of their structure and composition, as shown in Figs. 3(a) and 3(b). However, for very large molecules ($N \to \infty$), where the phoretic drift contributions of the absorbing–non-absorbing pairs are distributed randomly within a molecule, for statistical reasons, they scale with $N^{-1/2}$, where N is the number of monomers in the molecule. All molecules generally attract each other. For the laser power used in Fig. 1 (Multimedia view), these interactions are strong enough to bind colliding molecules together. However, for appropriate weaker attractions (at a lower laser power of only $I = 13\ \mu W\ \mu m^{-2}$), dimers do not grow towards larger molecules allowing to generate a gas containing only monomers and dimers.

## B. Theoretical model

To identify the key ingredients determining the emergence and dynamics of the colloidal molecules, we develop a phenomenological model based on the interplay of attractive (Lennard-Jones) interactions and particle diffusion inducing molecule formation, and the presence of nonreciprocal phoretic interactions creating self-propulsion of the molecules (see Appendix B for equations). The model describes a mixture of light-absorbing and non-absorbing overdamped Brownian (slightly soft) disks with radii $R = 0.49\ \mu m$ following overdamped Langevin dynamics including Gaussian white noise, which represents monomer diffusion and will automatically determine translational and rotational diffusion of the emerging molecules. We define the interactions among the individual colloids based on the following physical picture. Light-absorbing particles act as sources of phoretic fields (mainly temperature) in the near-critical binary liquid.[37,38,40] The gradients of these fields create a stress in the interfacial layer of all other colloids, which drives a solvent slip over their surfaces, leading to directed motion (phoresis) towards the absorbing particles.[27] Thus, light-absorbing particles attract each other reciprocally and non-reciprocally attract non-absorbing particles. In particular, when a non-absorbing particle closely approaches an absorbing one (distance 2R), it still experiences a gradient and pushes the absorbing particle forward, leading to directed motion of the absorbing–non-absorbing pair. (In addition, the non-absorbing particle displaces the relevant phoretic fields so that the absorbing particle itself experiences a phoretic gradient leading to phoretic motion; this can support its directed motion.) When several non-absorbing particles attach to an absorbing one, they collectively push it forward, i.e., the nonreciprocal "forces" in a corresponding molecule essentially superimpose determining, in competition with the overall drag force, the molecule's speed. Here, the involved phoretic fields might be effectively screened, e.g., due to heat-absorption processes or bulk-reactions[27] (unscreened phoretic attractions decaying quadratically with distance would provoke a rapid collapse of the system), so that their typical range extends over a few particle diameters. These interactions are supported by short-ranged attractions (van der Waals and perhaps critical Casimir interactions), which bind the particles in a molecule almost rigidly together. We phenomenologically model this using Lennard-Jones interactions, supplemented by nonreciprocal one-way attractions of non-absorbing particles by absorbing ones.

### 1. Speed and rotation rates

Here, we fix the strength of the nonreciprocal one-way attractions at contact distance (2R) by matching the dimer speed in our model (given by the non-reciprocal force at contact distance over Stokes drag force of the dimer) with experiments. The only remaining parameter to predict speed and rotation rates of all other molecules emerges from the fact that non-absorbing particles attaching to a molecule already containing non-absorbing particles (see a displaced phoretic field); thus, non-absorbing particles attaching adjacently to an absorbing one mutually reduce their contributions to the molecules' propulsion speed slightly. This reduction factor is fixed phenomenologically, as discussed in Appendix B. No further parameters are needed to predict the speed and the rotation rate of a given molecule, which can be done analytically in the absence of noise, based on force and torque balance equations (see Appendix B and the supplementary material). This allows us to predict the speed and rotation rates of all molecules in Fig. 3(a), quantitatively reproducing experiments.

### 2. Dynamics of molecule formation

To explore also the dynamics of molecule formation, we next perform Brownian dynamics simulations of our model. Here, we additionally account for the fact that nonabsorbing particles weakly attract each other in our experiments, if an absorbing particle is nearby. (In particular, they stay close to each other within a molecule rather than moving along the rim of an absorbing particle.) This weak attraction among nonabsorbing particles might result from a temperature dependence of the viscosity of the binary fluid, but could also involve, e.g., critical Casimir interactions activated by the absorbing colloids in the near-critical solvent. In our model, we account for these weak attractions by replacing excluded volume repulsions among nonabsorbing colloids with Lennard-Jones interactions with a small coefficient, if an absorbing particle is closer than a critical radius. (The choice of the coefficient and critical radius does not significantly influence the model's phenomenology.) Now simulating this model (see Appendix B for equations and details) using Brownian dynamics simulations, we observe the formation of active molecules as in the experiments, as shown by Figs. 1(e)–1(h) (Multimedia view): from a primordial broth of immotile single particles [Fig. 1(e) (Multimedia view)], first dimers form [Fig. 1(f) (Multimedia view)] and later grow into more complex active molecules [Fig. 1(g) (Multimedia view)]. Switching off the attractive interactions (corresponding to switching off the illumination in the experiment), the active molecules disassemble and their constituent particles diffuse away from each other [Fig. 1(h) (Multimedia view)]. Besides this qualitative agreement, our simulations allow us to extract the speed and rotation rates of the emerging molecules in the presence of Brownian noise (diffusion coefficient matched to experiments). Discretizing the simulated trajectory at 0.1 s (10 Hz), as in experiments, and then using finite differences to calculate speeds and swimming radii (i.e., speed over rotation frequency) allows for a quantitative comparison with experiments and our previous analytical calculations in the noise-free case. The blue circles in Fig. 3(a) represent experimentally measured speeds of various active molecules relative to the dimer speed, whereas red squares and black crosses show speed values found in analytical calculations and simulations, which are in quantitative agreement with the experimental results [Note that diffusion causes a finite speed even in perfectly symmetric molecules as can be seen in Fig. 3(a), right]. Blue circles in Fig. 3(b) represent the experimentally measured swimming radii $\rho$ of various chiral active molecules ($\rho = \infty$ for achiral molecules), whereas the red squares represent the corresponding swimming radii obtained from the simulations, which also agree broadly with the experimental results.

Our model applies to rather small molecules (up to about 10 monomers) and also to large molecules containing a low fraction of absorbing particles; for a high density of absorbing particles, in the experiments, the solvent heats up over an extended spatial region leading to a breakdown of the short-range attractions and to the emergence of repulsive forces between the absorbing and the non-absorbing particles.

## C. Controlling the clusters' behavior and functionality

The emergent behavior and functionality of this system can be controlled through a wealth of parameters. For example, in Fig. 3(c) we show that it is possible to change the fraction of achiral [e.g., Figs. 2(c)–2(e)] versus chiral [e.g., Figs. 2(g) and 2(h)] active molecules by changing the relative abundance of absorbing versus non-absorbing particles present in the initial suspension. The relative abundance of chiral active molecules increases with increasing deviation of the absorbing particle fraction from both 0 and 1. We can understand this result considering that only molecules featuring a common symmetry axis of composition and shape [Figs. 2(c)–2(e)] swim linearly, while molecules not featuring such a symmetry [Figs. 2(f) and 2(g)] are generally chiral (exceptions are molecules where rotational torques balance unsystematically); while such a symmetry is generally present for molecules consisting of only two or three individual colloids, all active molecules that break it involve at least two absorbing and two non-absorbing spheres. This latter requirement for being chiral is fulfilled for more molecules when the ratio of absorbing and non-absorbing colloids in the initial ensemble approaches 1/2. Also in this case, we find a good agreement between our experimental results [blue symbols in Fig. 3(c)] and the results of the simulations (red solid line). In fact, the simulations permit us to go beyond what can be realized experimentally as in experiments large assemblies including many absorbing colloids increase the temperature well beyond the critical point, inducing strong demixing around the colloids that prevents the formation of stable molecules involving attractive interactions. Also in this case, our simulations confirm the expectation described above, that the fraction of chiral to non-chiral molecules increases with increasing deviation of the fraction of absorbing to non-absorbing colloids from 1.

We can control the formation and growth of the molecules by tuning the light illumination. For example, it is possible to inhibit the formation of molecules larger than dimers by reducing the illumination to the minimum value ($I = 13\,\mu\mathrm{W}\,\mu\mathrm{m}^{-2}$) where attraction between absorbing and non-absorbing monomers still occurs: Monomers can easily bind to each other but not to dimers; when occasionally trimers emerge, they typically decay on timescales of a few seconds. For higher levels of illumination ($I > 20\,\mu\mathrm{W}\,\mu\mathrm{m}^{-2}$), the active molecules keep on growing in size indefinitely, if the illumination is constantly switched on. Despite this fact, we can control their size, shape, and functionality by subjecting them to periodic illumination. This is interesting because many natural phenomena are subject to periodic excitation (e.g., circadian rhythms, molecular clocks) and can be exploited to engineer artificial systems (e.g., autonomous nanorobots). For example, we can consider a periodic pattern of illumination where the illumination is alternatively switched on and off. Figure 4(a) (Multimedia view) shows that the active molecules that assemble when the light is periodically on for 5 s and off for 60 s are predominantly dimers and trimers, with few larger active molecules; this is in good agreement with simulations [Fig. 4(b) (Multimedia view)]. As the illumination time increases, the

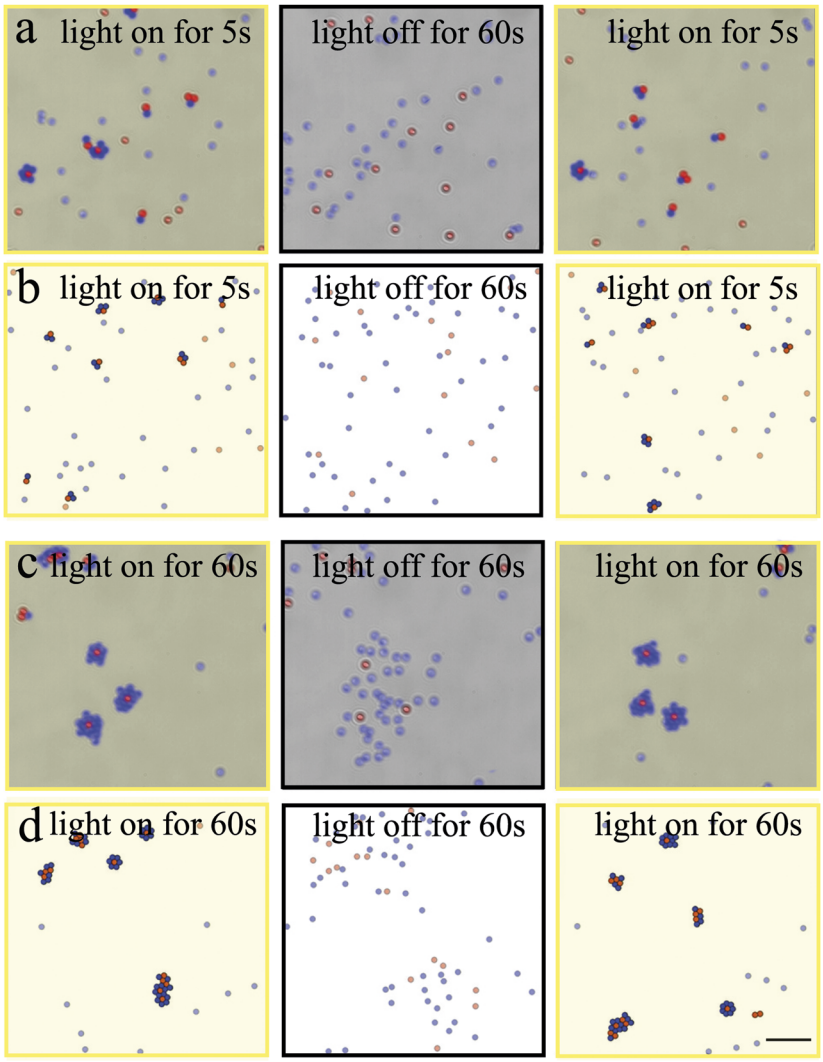


**FIG. 4. Controlling the assembly of active molecules by periodic illumination.** By subjecting the system to periodic illumination such that the light is periodically on for [(a) and (b)] 5 s and [(c) and (d)] 60 s and off always for 60 s, it is possible to assemble metastable active colloidal molecules with a controllable size, shape, and functionality, as their characteristic size increases with the light-on period. Each row features a series of three [(a) and (c)] experimental and [(b) and (d)] simulation snapshots taken at the end of a series of light-on, light-off, and light-on periods. Simulation parameters as in Fig. 1 (Multimedia view) and provided in Appendix B. The scale bar is 10 $\mu$m. Multimedia view: https://doi.org/10.1063/1.5079861.2

active molecules that form become larger and more complex and eventually will stop growing when the molecule has formed a large ring of non-absorbing particles around itself as shown in Fig. 4(c) (Multimedia view). Here, the light is periodically on for 60 s and off for 60 s, which is also in agreement with simulations [Fig. 4(d) (Multimedia view)].

## III. DISCUSSION

We have demonstrated the light-controlled assembly of active colloidal molecules starting from a mixture of different species of immotile building blocks. These molecules spontaneously acquire motility through non-reciprocal interactions of their immotile components and represent a new route to create active matter. Our proof-of-principle setup serves as a construction kit to assemble modular linear swimmers, migrators, spinners, and rotators with light-controllable shape, size, speed, and chirality. The table of the emerging active molecules and their characteristic properties can be quantitatively predicted by an effective model, which can be used in the future to design molecules and to predict their response to external fields, their large-scale collective behavior, and the properties of large molecules; the model may also be extended towards a more microscopic description[37,38] and to account for phoretic[46–49] and hydrodynamic interactions.[9,50] It will also be interesting to further explore the microscopic processes underlying the structure formation, explaining further how the structures are formed, how they can be controlled externally (e.g., by using spatiotemporal light modulators), and how individual molecules interact with each other. The exemplified route to create activity from immotile building blocks serves as a new design principle for active self-assembly. This might be useful both from a material perspective and to explore and design functionality in highly

controllable synthetic systems, which is so far often restricted to uncontrollable biological environments.

## SUPPLEMENTARY MATERIAL

See supplementary material for a figure of the phase diagram of the water-2,6-lutidine mixture, a schematic of the experimental setup, and further details on the model of the forces employed in the simulations as well as experimental and simulated videos of the snapshots provided in Figs. 1 (Multimedia view) and 4 (Multimedia view).

## ACKNOWLEDGMENTS

We thank C. Lozano for useful discussions. This work was partially supported by the ERC Starting Grant ComplexSwimmers (Grant No. 677511), Vetenskapsrådet (Grant No. 2016-03523), and the German Research Foundation DFG within LO 418–19-1.

## APPENDIX A: EXPERIMENTAL SETUP

We consider a suspension of colloidal particles in a critical mixture of water and 2,6-lutidine at the critical lutidine mass fraction $c_c = 0.286$ with a lower critical point at the temperature $T_c \approx 34\,^{\circ}\mathrm{C}$[51] (see Fig. S1 of the supplementary material). The light-absorbing species consists of silica microspheres with absorbing iron-oxide inclusions (Microparticles GmbH), while the non-absorbing species consists of equally sized plain silica microspheres (Microparticles GmbH). Both particle species have the same radius ($R = 0.49 \pm 0.03\ \mu$m) and similar density ($\rho \approx 2$ g cm$^{-3}$). The suspension is confined in a quasi-two-dimensional sample chamber realized between a microscope slide and a coverslip, where the particles sediment due to gravity.

A schematic of the setup is shown in Fig. S2 of the supplementary material. The motion of the particles is captured by digital video microscopy at 20 fps. Using a two-stage feedback temperature controller,[30,52] the temperature of the sample is adjusted to $T_0 = 31\,^{\circ}\mathrm{C}$, which is below $T_c$ so that water and 2,6-lutidine are homogeneously mixed. In these conditions, the microspheres of both species behave as independent immotile Brownian particles and undergo standard diffusion [Fig. 1(a) (Multimedia view)]. To illuminate the sample, we use a laser with a wavelength $\lambda = 532$ nm at an intensity $I = 80\ \mu\mathrm{W}\ \mu\mathrm{m}^{-2}$. The increase of temperature in the vicinity of the light-absorbing particles is rather small ($\Delta T \approx 4\,^{\circ}\mathrm{C}$) so that they still diffuse as normal (non-active) Brownian particles. This is reflected also by the trajectories for the light-absorbing and non-absorbing particles in Figs. 2(a) and 2(b).

## APPENDIX B: DETAILS OF THE MODEL

Following the physical picture discussed in the main text, (thermo-)phoretic interactions cause (i) mutual attractions among light-absorbing particles, (ii) nonreciprocal attractions of nonabsorbing particles towards absorbing particles (pushing them forward at close contact), and (iii) an additional phoretic drift of the absorbing particles when at close distance to a nonabsorbing particle, due to a displacement of the phoretic field by the latter, producing a gradient for the former. These phoretic effects are supported by short-range attractions among absorbing particles and particles in their vicinity (e.g., van der Waals and perhaps critical Casimir attractions in a near-critical solvent). Here, for simplicity, we phenomenologically model these effects as attractions between absorbing particles and all other particles, supplemented by a drift (nonreciprocal effective force) of absorbing-nonabsorbing pairs when in close distance (we assign these nonreciprocal forces to the absorbing particles; assigning them to the non-absorbing ones would equally work).

We now specifically define the model. To describe the dynamics of non-absorbing particles, we employ the following overdamped Langevin equation:[53]

$$\dot{\mathbf{r}}_i = -\frac{1}{\gamma}\sum_{j=1}^{N_a}\nabla_{\mathbf{r}_i}V_1(\mathbf{r}_i) - \frac{1}{\gamma}\sum_{j=1;j\neq i}^{N_p}\nabla_{\mathbf{r}_i}V_2(\mathbf{r}_i) + \sqrt{2D}\boldsymbol{\eta}_i(t)\,, \tag{B1}$$

where the left sum extends over all $N_a$ absorbing particles and the right one over all $N_p$ non-absorbing particles (excluding particle $i$), $\gamma$ is the Stokes drag coefficient (assumed to be independent from the distance to other particles), $D$ is the Brownian diffusion coefficient, and $\boldsymbol{\eta}_i$ represents Gaussian white noise with zero mean and unit variance.

The pair-interaction potential $V_1$ represents Lennard-Jones interactions acting between the absorbing and non-absorbing particles representing van der Waals and other attractions

$$V_1(\mathbf{r}_{ij}) = 4\epsilon\left[\left(\frac{\sigma}{r_{ij}}\right)^{12} - \left(\frac{\sigma}{r_{ij}}\right)^{6}\right], \tag{B2}$$

where we have used $r_{ij} = |\mathbf{r}_{ij}|$, $\mathbf{r}_{ij} = \mathbf{r}_i - \mathbf{r}_j$, and $\epsilon$ is the depth of the potential which crosses zero at $r = \sigma = 2R/\epsilon^{1/6}$. Note that the precise form of the interactions does not affect the set of emerging molecules or their speeds and rotation rates; attractive Yukawa interactions in combination with Weeks-Chandler Anderson repulsions basically lead to the same results. In our simulations, we choose a cutoff distance of $8R$ for the Lennard-Jones interactions; also this choice does not affect the molecules and their speeds and hardly affects the kinetics of molecule formation.

Conversely to interactions among pairs involving an absorbing particle, interactions among non-absorbing particles are purely repulsive. However, when an absorbing particle is in the vicinity of one of the non-absorbing particles (we phenomenologically choose a critical distance of $r_c = 8R$), it heats up the solvent locally, leading to relatively weak attractions among the colloids. We therefore model the interactions among the non-absorbing particles as

$$\nabla_{\mathbf{r}_i}V_2(\mathbf{r}_{ij}) = \begin{cases} \nabla_{\mathbf{r}_i}V_1(\mathbf{r}_{ij}) & r_{ij} \le 2R \\ \alpha\nabla_{\mathbf{r}_i}V_1(\mathbf{r}_{ij}) & r_{ij} > 2R \ \text{ and} \\ & \sum_{k=1}^{N_a}\theta\left(r_c - \max(r_{ik}, r_{jk})\right) > 0 \\ 0 & \text{otherwise,} \end{cases} \tag{B3}$$

where $\alpha \ll 1$ determines the relative interaction strength among non-absorbing particles compared to the interaction strength among absorbing particles. The key effect of the attractions among non-absorbing colloids in the vicinity of an absorbing one is that they tend to stay next to each other within a molecule, rather than moving almost freely along the rim of an absorbing particle.

When the laser is switched off, all particles are non-absorbing; however, when the laser is switched on, we describe the dynamics of absorbing particles by the following Langevin equation:

$$\dot{\mathbf{r}}_i = -\frac{1}{\gamma}\sum_{j=1;j\neq i}^{N} \nabla_{\mathbf{r}_i} V_1(\mathbf{r}_i) + \sum_{j=1}^{N_p} \mathbf{v}_{ij} + \sqrt{2D}\boldsymbol{\eta}_i(t)\,, \tag{B4}$$

where we have introduced the phoretic drift velocity $\mathbf{v}_{ij} = v_{ij}\theta(r_p - r_{ij})\mathbf{r}_{ij}/r_{ij}^3$ describing the directed motion of non-absorbing particle $i$ due to absorbing particle $j$. These drift terms represent the nonreciprocal contribution to the interaction of absorbing and nonabsorbing particles, and $\mathbf{F}_i = \gamma\sum_{j=1}^{N_p}\mathbf{v}_{ij}$ is the corresponding nonreciprocal force acting on particle $i$. Here, the values of $v_{ij}$ at contact distance $2R$ (see below) determine the speed and rotation rates of the molecules; the $1/r^2$-scaling and the cutoff at $r_p = 2.8R$ are arbitrary choices leading to a smooth onset of directed motion. Physically, such a directed motion occurs because gradients in the phoretic fields that the absorbing particles produce induce a stress in the interfacial layers of the non-absorbing particles leading to a localized solvent flow across their surface; this flow induces a directed motion of the non-absorbing particles towards the absorbing ones. When in close contact, the non-absorbing particles push the absorbing particles forward; at the same time, they displace the phoretic fields produced by the absorbing particles, which induces a phoretic motion of the absorbing particles themselves. Both effects lead to a directed motion of the absorbing–non-absorbing pairs.

Finally, we use the following expression for the coefficient of the phoretic velocity:

$$v_{ij} = v_0\left[1 - \frac{1}{6}\sum_{k=1,k\neq j}^{N_p}\theta(r_c - r_{jk})\right], \tag{B5}$$

where $v_0$ determines the propulsion speed of an isolated absorbing–non-absorbing pair as $v_0/(8R^2)$. The term in square brackets accounts for the fact that adjacent non-absorbing particles attached to an absorbing one do not contribute fully independently to the propulsion-speed but mutually suppress their contributions slightly. This is partly caused by the fact that each non-absorbing particle displaces the phoretic field produced by an absorbing particle so that each additional non-absorbing particle attaching to an absorbing one sees a different phoretic field. This may be viewed as a mutual shielding of a part of the absorbing colloid's surface. Here, we phenomenologically assume that each non-absorbing particle covers an angle of $\theta = \pi/2$ (2D projection) of the surface of the absorbing colloids [see Fig. 3(a) of the supplementary material]. Thus, when two non-absorbing colloids adjacently attach to an absorbing colloid, the areas they cover overlap by an angle of $\theta_0 = \pi/6$ [see Fig. 3(b) of the supplementary material], reducing $v_0 \to 5v_0/6$. Analogously, the contribution of a non-absorbing colloid in between two other ones is reduced by a factor of 1/3. This is represented by the sum in Eq. (B5), where $r_c$ is an arbitrary value which must be chosen slightly larger than $2R$ (here $r_c = 2.3R$).

### 1. Choice of parameters

Here, we provide the parameters we used in the implementation of the simulations. As discussed in the main text, the speed and the rotation rate can be predicted based on two parameters, the dimer speed (or $v_0$) and the "shielding" angle $\theta$ (set to $\pi/2$ above) alone. Other parameters, most of which can be extracted from experiments, are relevant only to understand the dynamics of molecule formation. To allow for a straightforward comparison with experiments, we use 1 $\mu$m and 1 s as length and time units in all the simulations. For Figs. 1 (Multimedia view) and 4 (Multimedia view), we have used $R = 0.49\ \mu$m and $D = 0.1\ \mu\text{m}^2\ \text{s}^{-1}$. We have further chosen $\epsilon/\gamma = 10$, i.e., $\epsilon/(kT) = 100$, so that the molecules, once formed, are robust against thermal fluctuations, as in the experiments. We use $v_0 = 24R^2$ yielding a dimer speed of $\approx$3, or 3 $\mu$m/s, similar as in experiments. Finally, choosing $\alpha = 1/20$ yields a comparatively weak mutual attraction among non-absorbing particles [strength $\epsilon/(kT) = 5$], if an absorbing one is close by. In Fig. 3, which shows the molecule speed normalized by the pair speed, the absolute value of the propulsion speed is unimportant; here, we have chosen $v_0 = 80R^2$ for efficiency of the simulations. We have further used $R = 0.49\ \mu$m, $\epsilon/\gamma = 500$, and $\alpha = 1$ to strongly avoid fluctuations of the molecule shapes in the course of a simulation. Finally, we have used a somewhat stronger diffusion $D = 0.41\ \mu\text{m}^2\ \text{s}^{-1}$ [Figs. 3(a) and 3(b)] and $D = 0.195\ \mu\text{m}^2\ \text{s}^{-1}$ [Fig. 3(c)] to accelerate molecule formation and the corresponding convergence of ensemble averages; here, noise is largely negligible (for the used sampling rate) as can be seen from the comparisons with the noise-free analytical calculations of the relative speed and rotation rates of the molecules which are practically identical to the simulated ones [Figs. 3(a) and 3(c)].

### 2. Analytical predictions of speed and rotation frequency of molecules

The speed, rotation radius, and reorientation frequency of a given molecule can be calculated analytically in the zero-noise limit by assuming hexagonal close packing within the molecule. Consider the molecule as a rigid body and the following balance conditions for the effective nonreciprocal forces $\mathbf{F}_i := \gamma\sum_{j=1}^{N_p}\mathbf{v}_{ij}$, evaluated at contact distance $2R$ ($\mathbf{F}_i = 0$ for non-absorbing particles), and the associated effective torques

$$\sum_{i=1}^{N}\mathbf{F}_i - \gamma\dot{\mathbf{r}}_i = 0, \quad \sum_{i=1}^{N}(\mathbf{r}_i - \mathbf{R})\times(\mathbf{F}_i - \gamma\dot{\mathbf{r}}_i) = 0\,, \tag{B6}$$

where we sum over all N particles in a molecule and choose **R** as the centre of mass of the molecule. From here, using polar coordinates, we readily find the considered molecule's velocity and rotation frequency as

$$\mathbf{v} = \dot{\mathbf{R}} = \frac{1}{N\gamma}\sum_{i=1}^{N}\mathbf{F}_i \tag{B7}$$

and

$$\omega = \frac{1}{\gamma}\left|\frac{\sum_{i=1}^{N}\mathbf{x}_i \times \mathbf{F}_i}{\sum_{i=1}^{N}\mathbf{x}_i^2}\right|, \tag{B8}$$

where $\mathbf{x}_i$ is the relative coordinate of sphere $i$ with respect to the centre of mass of the active molecule. From Eq. (B8), the gyration radius $\rho$ follows as $\rho = \frac{|\mathbf{v}|}{\omega}$. In Fig. 3(c) of the supplementary material, we exemplarily illustrate the analytical calculation of the swimming speed and swimming radius for a molecule consisting of 5 particles (2 absorbing and 3 non-absorbing).

## REFERENCES


[1] V. N. Manoharan, M. T. Elsesser, and D. J. Pine, "Dense packing and symmetry in small clusters of microspheres," Science **301**, 483–487 (2003).
[2] E. Bianchi, J. Largo, P. Tartaglia, E. Zaccarelli, and F. Sciortino, "Phase diagram of patchy colloids: Towards empty liquids," Phys. Rev. Lett. **97**, 168301 (2006).
[3] Y. Wang, Y. Wang, D. R. Breed, V. N. Manoharan, L. Feng, A. D. Hollingsworth, M. Weck, and D. J. Pine, "Colloids with valence and specific directional bonding," Nature **491**, 51–55 (2012).
[4] T. A. Nguyen, A. Newton, D. J. Kraft, P. G. Bolhuis, and P. Schall, "Tuning patchy bonds induced by critical Casimir forces," Materials **10**, 1265 (2017).
[5] R. Niu, T. Palberg, and T. Speck, "Self-assembly of colloidal molecules due to self-generated flow," Phys. Rev. Lett. **119**, 028001 (2017).
[6] R. Niu, D. Botin, J. Weber, A. Reinmüller, and T. Palberg, "Assembly and speed in ion-exchange-based modular phoretic microswimmers," Langmuir **33**, 3450–3457 (2017).
[7] S. Ramaswamy, "The mechanics and statistics of active matter," Annu. Rev. Condens. Matter Phys. **1**, 323–345 (2010).
[8] A. M. Menzel, "Tuned, driven, and active soft matter," Phys. Rep. **554**, 1–45 (2015).
[9] A. Zöttl and H. Stark, "Emergent behavior in active colloids," J. Phys.: Condens. Matter **28**, 253001 (2016).
[10] C. Bechinger, R. Di Leonardo, H. Löwen, C. Reichhardt, G. Volpe, and G. Volpe, "Active particles in complex and crowded environments," Rev. Mod. Phys. **88**, 045006 (2016).
[11] F. Peruani, A. Deutsch, and M. Bär, "Nonequilibrium clustering of self-propelled rods," Phys. Rev. E **74**, 030904 (2006).
[12] D. B. Dusenbery, *Living at Micro Scale: The Unexpected Physics of Being Small* (Harvard University Press, 2009).
[13] R. Trask, H. Williams, and I. Bond, "Self-healing polymer composites: Mimicking nature to enhance performance," Bioinspiration Biomimetics **2**, P1 (2007).
[14] H. P. Narra and H. Ochman, "Of what use is sex to bacteria?," Curr. Biol. **16**, R705–R710 (2006).
[15] A. Ivlev, J. Bartnick, M. Heinen, C.-R. Du, V. Nosenko, and H. Löwen, "Statistical mechanics where Newton's third law is broken," Phys. Rev. X **5**, 011035 (2015).
[16] R. Soto and R. Golestanian, "Self-assembly of catalytically active colloidal molecules: Tailoring activity through surface chemistry," Phys. Rev. Lett. **112**, 068301 (2014).
[17] R. Soto and R. Golestanian, "Self-assembly of active colloidal molecules with dynamic function," Phys. Rev. E **91**, 052304 (2015).
[18] M. Popescu, M. Tasinkevych, and S. Dietrich, "Pulling and pushing a cargo with a catalytically active carrier," Europhys. Lett. **95**, 28004 (2011).
[19] L. Baraban, M. Tasinkevych, M. N. Popescu, S. Sanchez, S. Dietrich, and O. Schmidt, "Transport of cargo by catalytic Janus micro-motors," Soft Matter **8**, 48–52 (2012).
[20] J. Zhang, J. Yan, and S. Granick, "Directed self-assembly pathways of active colloidal clusters," Angew. Chem., Int. Ed. **55**, 5166 (2016).
[21] D. P. Singh, U. Choudhury, P. Fischer, and A. G. Mark, "Non-equilibrium assembly of light-activated colloidal mixtures," Adv. Mater. **29**, 1701328 (2017).
[22] S. Ilday, G. Makey, G. B. Akguc, Ö. Yavuz, O. Tokel, I. Pavlov, O. Gülseren, and F. Ö. Ilday, "Rich complex behaviour of self-assembled nanoparticles far from equilibrium," Nat. Commun. **8**, 14942 (2017).
[23] H. Löwen, "Active colloidal molecules," Europhys. Lett. **121**, 58001 (2018).
[24] F. Ma, S. Wang, D. T. Wu, and N. Wu, "Electric-field–induced assembly and propulsion of chiral colloidal clusters," Proc. Natl. Acad. Sci. U. S. A. **112**, 6307 (2015).
[25] F. Ma, X. Yang, H. Zhao, and N. Wu, "Inducing propulsion of colloidal dimers by breaking the symmetry in electrohydrodynamic flow," Phys. Rev. Lett. **115**, 208302 (2015).
[26] J. Palacci, S. Sacanna, A. P. Steinberg, D. J. Pine, and P. M. Chaikin, "Living crystals of light-activated colloidal surfers," Science **339**, 936 (2013).
[27] B. Liebchen and H. Löwen, "Which interactions dominate in active colloids?," preprint arxiv:1808.07389 (2018).
[28] T. Yu, P. Chuphal, S. Thakur, S. Y. Reigh, D. P. Singh, and P. Fischer, "Chemical micromotors self-assemble and self-propel by spontaneous symmetry breaking," Chem. Commun. **54**, 11933 (2018).
[29] C. Hertlein, L. Helden, A. Gambassi, S. Dietrich, and C. Bechinger, "Direct measurement of critical Casimir forces," Nature **451**, 172 (2008).
[30] S. Paladugu, A. Callegari, Y. Tuna, L. Barth, S. Dietrich, A. Gambassi, and G. Volpe, "Nonadditivity of critical Casimir forces," Nat. Commun. **7**, 11403 (2016).
[31] V. Nguyen, M. Dang, T. Nguyen, and P. Schall, "Critical Casimir forces for colloidal assembly," J. Phys.: Condens. Matter **28**, 043001 (2016).
[32] J. L. Anderson, "Colloid transport by interfacial forces," Annu. Rev. Fluid Mech. **21**, 61–99 (1989).
[33] R. Golestanian, T. B. Liverpool, and A. Ajdari, "Propulsion of a molecular machine by asymmetric distribution of reaction products," Phys. Rev. Lett. **94**, 220801 (2005).
[34] G. Volpe, I. Buttinoni, D. Vogt, H.-J. Kümmerer, and C. Bechinger, "Microswimmers in patterned environments," Soft Matter **7**, 8810 (2011).
[35] I. Buttinoni, G. Volpe, F. Kümmel, G. Volpe, and C. Bechinger, "Active Brownian motion tunable by light," J. Phys.: Condens. Matter **24**, 284129 (2012).
[36] F. Kümmel, B. ten Hagen, R. Wittkowski, I. Buttinoni, R. Eichhorn, G. Volpe, H. Löwen, and C. Bechinger, "Circular motion of asymmetric self-propelling particles," Phys. Rev. Lett. **110**, 198302 (2013).
[37] A. Würger, "Self-diffusiophoresis of Janus particles in near-critical mixtures," Phys. Rev. Lett. **115**, 188304 (2015).
[38] S. Samin and R. Van Roij, "Self-propulsion mechanism of active Janus particles in near-critical binary mixtures," Phys. Rev. Lett. **115**, 188305 (2015).
[39] I. Theurkauff, C. Cottin-Bizonne, J. Palacci, C. Ybert, and L. Bocquet, "Dynamic clustering in active colloidal suspensions with chemical signaling," Phys. Rev. Lett. **108**, 268303 (2012).
[40] I. Buttinoni, J. Bialké, F. Kümmel, H. Löwen, C. Bechinger, and T. Speck, "Dynamical clustering and phase separation in suspensions of self-propelled colloidal particles," Phys. Rev. Lett. **110**, 238301 (2013).
[41] P. H. Colberg and R. Kapral, "Nanoconfined catalytic Angström-size motors," J. Chem. Phys. **143**, 184906 (2015).
[42] S. H. Klapp, "Collective dynamics of dipolar and multipolar colloids: From passive to active systems," Curr. Opin. Colloid Interface Sci. **21**, 76–85 (2016).

[43]S. Ebbens, "Active colloids: Progress and challenges towards realising autonomous applications," Curr. Opin. Colloid Interface Sci. **21**, 14–23 (2016).
[44]M. C. Marchetti, Y. Fily, S. Henkes, A. Patch, and D. Yllanes, "Minimal model of active colloids highlights the role of mechanical interactions in controlling the emergent behavior of active matter," Curr. Opin. Colloid Interface Sci. **21**, 34–43 (2016).
[45]J. Happel and H. Brenner, *Low Reynolds Number Hydrodynamics* (Springer Science & Business Media, 2012), Vol. 1.
[46]S. Saha, R. Golestanian, and S. Ramaswamy, "Clusters, asters, and collective oscillations in chemotactic colloids," Phys. Rev. E **89**, 062316 (2014).
[47]O. Pohl and H. Stark, "Dynamic clustering and chemotactic collapse of self-phoretic active particles," Phys. Rev. Lett. **112**, 238303 (2014).
[48]B. Liebchen, D. Marenduzzo, I. Pagonabarraga, and M. Cates, "Clustering and pattern formation in chemorepulsive active colloids," Phys. Rev. Lett. **115** (2015).
[49]B. Liebchen, D. Marenduzzo, and M. E. Cates, "Phoretic interactions generically induce dynamic clusters and wave patterns in active colloids," Phys. Rev. Lett. **118**, 268001 (2017).
[50]S. C. Takatori and J. F. Brady, "Forces, stresses and the (thermo?) dynamics of active matter," Curr. Opin. Colloid Interface Sci. **21**, 24–33 (2016).
[51]C. A. Grattoni, R. A. Dawe, C. Y. Seah, and J. D. Gray, "Lower critical solution coexistence curve and physical properties (density, viscosity, surface tension, and interfacial tension) of 2,6-lutidine + water," J. Chem. Eng. Data **38**, 516 (1993).
[52]F. Schmidt, A. Magazzù, A. Callegari, L. Biancofiore, F. Cichos, and G. Volpe, "Microscopic engine powered by critical demixing," Phys. Rev. Lett. **120**, 068004 (2018).
[53]G. Volpe, S. Gigan, and G. Volpe, "Simulation of the active Brownian motion of a microswimmer," Am. J. Phys. **82**, 659–664 (2014).